Reflected Shock Tube Studies of High-Temperature Rate Constants for OH + NO$_2$ → HO$_2$ + NO and OH + HO$_2$ → H$_2$O + O$_2$[†]

Nanda K. Srinivasan,[‡] Meng-Chih Su,[‡,§] James W. Sutherland,[‡,||] Joe V. Michael,*[,‡] and Branko Ruscic[‡]

Chemistry Division, Argonne National Laboratory, Argonne, Illinois 60439-4831

Received: December 22, 2005; In Final Form: February 9, 2006

The motivation for the present study comes from the preceding paper where it is suggested that accepted rate constants for OH + NO$_2$ → NO + HO$_2$ are high by ~2. This conclusion was based on a reevaluation of heats of formation for HO$_2$, OH, NO, and NO$_2$ using the Active Thermochemical Table (ATcT) approach. The present experiments were performed in C$_2$H$_5$I/NO$_2$ mixtures, using the reflected shock tube technique and OH-radical electronic absorption detection (at 308 nm) and using a multipass optical system. Time-dependent profile decays were fitted with a 23-step mechanism, but only OH + NO$_2$, OH + HO$_2$, both HO$_2$ and NO$_2$ dissociations, and the atom molecule reactions, O + NO$_2$ and O + C$_2$H$_4$, contributed to the decay profile. Since all of the reactions except the first two are known with good accuracy, the profiles were fitted by varying only OH + NO$_2$ and OH + HO$_2$. The new ATcT approach was used to evaluate equilibrium constants so that back reactions were accurately taken into account. The combined rate constant from the present work and earlier work by Glaenzer and Troe (GT) is $k_{\text{OH+NO}_2}$ = 2.25 × 10^{-11} exp(−3831 K/*T*) cm^3 molecule^{-1} s^{-1}, which is a factor of 2 lower than the extrapolated direct value from Howard but agrees well with NO + HO$_2$ → OH + NO$_2$ transformed with the updated equilibrium constants. Also, the rate constant for OH + HO$_2$ suitable for combustion modeling applications over the *T* range (1200−1700 K) is (5 ± 3) × 10^{-11} cm^3 molecule^{-1} s^{-1}. Finally, simulating previous experimental results of GT using our updated mechanism, we suggest a constant rate for $k_{\text{HO}_2+\text{NO}_2}$ = (2.2 ± 0.7) × 10^{-11} cm^3 molecule^{-1} s^{-1} over the *T* range 1350−1760 K.

1. Introduction

In kinetics studies[1] of the reactions, NO + HO$_2$ → OH + NO$_2$, and its reverse over the respective temperature ranges of 232−1271 K and 452−1115 K, the heat of formation at 298 K for HO$_2$ radicals was determined to be 2.5 ± 0.6 kcal mol^{-1}, implying $\Delta_f H_0^\circ$ = 3.2 ± 0.6 kcal mol^{-1}. This value was accepted by most workers and was a large change from the values recommended in the JANAF compilation ($\Delta_f H_{298}^\circ$ = 0.5 ± 2.0 and $\Delta_f H_0^\circ$ = 1.2 ± 2.0, both in kcal mol^{-1}).[2] As thoroughly discussed in the preceding article in this volume,[3] later experiments and evaluations caused significant fluctuations in this heat of formation. The preferred values, as assessed with the Active Thermochemical Table (ATcT) procedure,[3] are now $\Delta_f H_{298}^\circ$ = 2.94 ± 0.06 and $\Delta_f H_0^\circ$ = 3.64 ± 0.06, both again being in kcal mol^{-1}. We noted[3] that the 0.44 kcal mol^{-1} change from the Howard value would then suggest that either the measured NO + HO$_2$ rate constant was low by ~2 or the measured OH + NO$_2$ rate constant was high by ~2. Since the NO + HO$_2$ reaction is of major importance in stratospheric ozone depletion,[4] this rate constant has been measured several times.[5−10] The values at room temperature range between 6.1

and 9.5 with the mean value being 7.9 × 10^{-11} cm^3 molecule^{-1} s^{-1}. The temperature dependence was measured in two of the studies,[1,9] and the agreement was excellent over the overlapping temperature range. There can be no doubt that the NO + HO$_2$ rate constants are accurate from 206 to 1271 K. Hence, the reported rate constants for the reverse reaction, OH + NO$_2$, are incompatible with the updated $\Delta_f H_0^\circ$ for HO$_2$, and this supplies the motivation for the present study.

2. Experimental Section

2.1. Approach. We described earlier a long absorption path multipass optical system for OH-radical detection in the reflected shock waves[11,12] and used it to measure high-temperature rate constants.[11,13,14] With a path length of 2.798 m, high sensitivity for OH-radical detection is possible thereby minimizing the effects of secondary reaction perturbations. In this work, the same method used previously was employed. OH-radicals were generated by the H + NO$_2$ reaction[13] from controlled H-atom formation using C$_2$H$_5$I decomposition,[15] that is,

$$C_2H_5I \ (+ \ M) \rightarrow C_2H_4 + H + I \ (+ \ M) \qquad (1)$$

$$C_2H_5I \ (+ \ M) \rightarrow C_2H_4 + HI \ (+ \ M) \qquad (2)$$

$$H + NO_2 \rightarrow OH + NO \qquad (3)$$
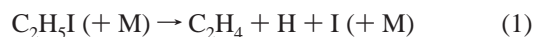
Reaction 1 is composite since the initially formed C$_2$H$_5$ radicals instantaneously decompose under the present high-temperature conditions. If [NO$_2$] is large, then reaction 3 is likewise nearly

Shock Tube Studies for Bimolecular Reactions

*J. Phys. Chem. A, Vol. 110, No. 21, 2006* **6603**

instantaneous. Therefore, the thermal decomposition of C_2H_5I controls the rate of formation of OH. If the temperature is high enough so that the thermal decomposition is fast, then a pulse of OH at short times is formed, and this property was then used to obtain the temperature dependence of the absorption cross section.[11] Clearly, if [NO_2] is in large enough excess, the effects of the OH + NO_2 reaction should be reflected in the OH-radical concentration profile, and with this strategy, a decision on the abovementioned incompatibility between forward and reverse rates may be possible.

2.2. Instrumentation. The present experiments were performed with the shock tube technique using OH-radical electronic absorption detection. The method and the apparatus currently being used have been previously described,[16,17] and only a brief description of the experiment will be presented here.

The shock tube is constructed from 304 stainless steel in three sections. The first 10.2 cm-o.d. cylindrical section is separated from the He driver chamber by a 4 mil unscored 1100-H18 aluminum diaphragm. A 0.25 m transition section then connects the first and third sections. The third section is of rounded corner (radius, 1.71 cm) square design and is fabricated from flat stock (3 mm) with a mirror finish. The tube length is 7 m, and the driver to driven volume ratio is about 3:1.[18] Two sets of flat fused silica windows (3.81 cm) with broadband antireflection (BB AR) coating for UV light are mounted on the tube across from one another at a distance of 6 cm from the end plate. The path length between windows is 8.745 cm. The incident shock velocity is measured with eight fast pressure transducers (PCB Piezotronics, Inc., Model 113A21) mounted along the third portion of the shock tube, and temperature and density in the reflected shock wave regime are calculated from this velocity and include corrections for boundary layer perturbations.[18-21] Because the tube is long, the shock waves do not attenuate (giving constant velocities) with the loading pressures used in this investigation. The tube is routinely pumped between experiments to $<10^{-8}$ Torr by an Edwards Vacuum Products Model CR100P packaged pumping system. A 4094C Nicolet digital oscilloscope was used to record both the velocity and absorption signals.

The optical configuration consists of an OH resonance lamp,[11,13,22] multipass reflectors, an interference filter at 308 nm, and a photomultiplier tube (1P28) all mounted external to the shock tube as described previously.[11,13] At the entrance to the multipass cell, the resultant OH resonance radiation was collimated with a set of lenses and was focused onto the reflector on the opposite side of the shock tube through two AR coated windows that were flush mounted to the inside of the shock tube. The reflectors and windows were obtained from the CVI Laser Corporation. These reflectors were attached to adjustable mounts, and the center points of windows and mirrors were all in a coaxial position. With this new configuration, we were able to obtain 32 passes, giving a total path length of 2.798 m, thereby amplifying the measured absorbances. Thus, a substantially better sensitivity (at least a factor of 2) is achieved for OH-radical detection than in the previous work.[13,22] In these experiments, particularly at the higher pressures, zero time can only be determined to within $\sim \pm 10$ μs due to schlieren interference.

2.3. Gases. High-purity He (99.995%), used as the driver gas, was from AGA Gases. Scientific grade Kr (99.999%), the diluent gas in reactant mixtures, was from Spectra Gases, Inc. The $\sim$10 ppm impurities (N_2, 2 ppm; O_2, 0.5 ppm; Ar, 2 ppm; CO_2, 0.5 ppm; H_2, 0.5 ppm; CH_4, 0.5 ppm, H_2O, 0.5 ppm; Xe, 5 ppm; CF_4, 0.5 ppm) are all either inert or in sufficiently low
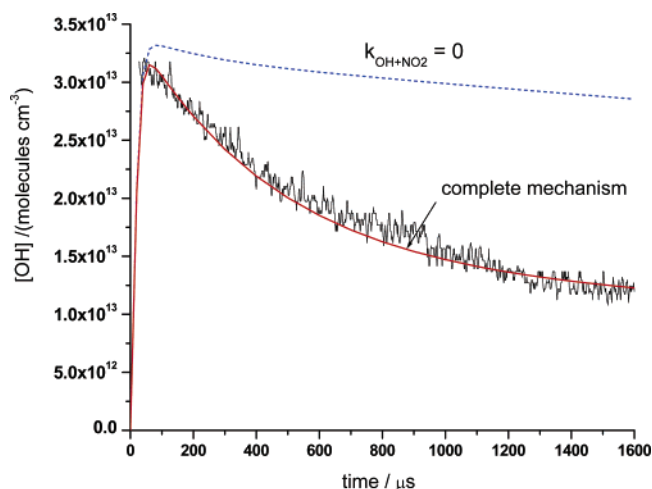
Figure 1. Sample temporal profile of OH absorption: solid line, fit with the reaction model of Table 1; dashed line, simulation with the full model but with $k_{OH+NO_2} = 0$. $P_1 = 30.58$ Torr and $M_s = 2.430$. $T_5 = 1461$ K, $\rho_5 = 5.588 \times 10^{18}$ molecules cm^{-3}, [NO_2]$_0 = 5.672 \times 10^{14}$ molecules cm^{-3}, and [C_2H_5I] $= 3.915 \times 10^{13}$ molecules cm^{-3}.

concentration so as to not perturb the OH-radical profiles. Distilled water, evaporated at 1 atm into ultrahigh purity grade Ar (99.999%) from AGA Gases, was used at $\sim$25 Torr pressure in the resonance lamp. Analytical grade C_2H_5I (99%), from Aldrich Chemical Co. Inc., and technical grade NO_2, from Matheson Gas Products, were further purified by bulb-to-bulb distillations with the middle thirds being retained. Test gas mixtures were accurately prepared from pressure measurements using a Baratron capacitance manometer and were stored in an all-glass vacuum line.

3. Results and Discussion

3.1. Kinetics. In this work, the temporal concentration profiles of OH radicals were measured after the initial [OH] pulse generated by eqs 1−3. A typical OH profile is shown in Figure 1 where the concentration is seen to slowly decay as time increases. Uncertainty due to schlieren interference has a minimal effect on the slow long-time temporal profile. This long-time behavior was noted previously[13] and was attributed to OH-radical termination by the self-reaction, OH + OH → H_2O + O. However, this reaction has been studied both directly[23] and with O + H_2O → OH + OH transformed through equilibrium constants.[16] With the recent reevaluation for the heat of formation for OH radicals,[24,25] the direct and transformed rate constants now agree with one another, over the present temperature range, 1237−1554 K, to within <8%, and hence, this rate constant is accurately known. Including eqs 1−3 and the self-reaction in an extended mechanism shows that the decreasing [OH]$_t$ behavior is not due to the self-reaction. We tested other possible causes (e.g., OH + C_2H_4) eventually building the 15 species−23-step mechanism shown in Table 1.[26-35] With the low [OH] used in the present study, only a few radical−radical and radical−molecule bimolecular reactions are important as illustrated in the [OH] sensitivity plot shown in Figure 2. [OH]$_t$ is most sensitive to OH + NO_2 with significant contributions from OH + HO_2, both HO_2 and NO_2 dissociations, and the atom molecule reactions, O + NO_2 and O + C_2H_4.

Before reliable rate constants can be derived from profile fits, the accuracy of the sensitive secondary processes should be considered. Earlier values for HO_2 dissociation in N_2 vary by $\sim$2 with Tsang and Hampson[36] being lower than either the GRI

TABLE 1: Mechanism for Determining [OH]$_t$

reaction	rate constant^a	ref
$C_2H_5I \, (+ \, Kr) \rightarrow C_2H_4 + H + I + Kr$	$k_1 = 6.34 \times 10^9 \exp(-15894 \, K/T)$	15
$C_2H_5I + Kr \rightarrow C_2H_4 + HI + Kr$	$k_2 = 0.15 \times k_1$	15
$H + NO_2 \rightarrow OH + NO$	$k_3 = 1.47 \times 10^{-10}$	13
$H + HI \rightarrow H_2 + I$	$k_4 = 9.29 \times 10^{-11} \exp(-59 \, K/T)$	26
$H_2 + I \rightarrow H + HI$	$k_5 = 4.52 \times 10^{-10} \exp(-17070 \, K/T)$	26
$OH + OH \rightarrow O + H_2O$	$k_6 = 7.19 \times 10^{-21} \, T^{2.7} \exp(917 \, K/T)$	16, 23, 24
$O + H_2O \rightarrow OH + OH$	$k_7 = 7.48 \times 10^{-20} \, T^{2.7} \exp(-7323 \, K/T)$	16, 23, 24
$H + O_2 \rightarrow OH + O$	$k_8 = 1.62 \times 10^{-10} \exp(-7474 \, K/T)$	27
$OH + O \rightarrow O_2 + H$	$k_9 = 5.42 \times 10^{-13} \, T^{0.375} \exp(950 \, K/T)$	16, 24, 27
$O + H_2 \rightarrow OH + H$	$k_{10} = 8.44 \times 10^{-20} \, T^{2.67} \exp(-3167 \, K/T)$	16, 24
$OH + H \rightarrow H_2 + O$	$k_{11} = 3.78 \times 10^{-20} \, T^{2.67} \exp(-2393 \, K/T)$	16, 24
$OH + H_2 \rightarrow H_2O + H$	$k_{12} = 3.56 \times 10^{-16} \, T^{1.52} \exp(-1736 \, K/T)$	28
$H_2O + H \rightarrow OH + H_2$	$k_{13} = 1.56 \times 10^{-15} \, T^{1.52} \exp(-9083 \, K/T)$	16, 24, 28
$NO_2 + Kr \rightarrow NO + O + Kr$	$k_{14} = 6.61 \times 10^{-9} \exp(-30189 \, K/T)$	29
$NO_2 + O \rightarrow NO + O_2$	$k_{15} = 4.21 \times 10^{-12} \exp(273 \, K/T)$	30
$OH + C_2H_4 \rightarrow H_2O + H + C_2H_2$	$k_{16} = 3.35 \times 10^{-11} \exp(-2990 \, K/T)$	31
$O + C_2H_4 \rightarrow H + C_2H_3O$	$k_{17} = (0.39 \exp(-123 \, K/T)) \times (2.25 \times 10^{-17} \, T^{1.88} \exp(-92 \, K/T))$	32, 33
$O + C_2H_4 \rightarrow OH + H + C_2H_2$	$k_{18} = (1-0.39 \exp(-123 \, K/T)) \times (2.25 \times 10^{-17} \, T^{1.88} \exp(-92 \, K/T))$	32, 33
$OH + NO_2 \rightarrow NO + HO_2$	$k_{19} = $ to be fitted	
$NO + HO_2 \rightarrow OH + NO_2$	$k_{20} = k_{19} \, (0.229731 \exp(3571 \, K/T))$	
$HO_2 + Kr \rightarrow H + O_2 + Kr$	$k_{21} = 7.614 \times 10^{-10} \exp(-22520 \, K/T)$	34
$OH + HO_2 \rightarrow O_2 + H_2O$	$k_{22} = $ to be fitted	
$I + HO_2 \rightarrow HI + O_2$	$k_{23} = 1.47 \times 10^{-11} \exp(-1090 \, K/T)$	35

^{a} All rate constants are in units cm^3 molecule^{-1} s^{-1}.

Mech[37] or Leeds[38] databases. The reverse reaction in seven bath gases including Kr was recently studied in this laboratory.[34] In that work, the relative collision efficiencies were determined, and new and existing third-order rate constant determinations were reviewed and fitted with a theoretical model. The values, from transformations through equilibrium constants, for HO_2 dissociation in N_2 were 10−20% higher than Tsang and Hampson, 35−55% lower than GRI Mech, and 70−110% lower than Leeds. The success of the model for a variety of bath gases[34] leads us to prefer, over the present experimental temperature range, the transformed rate constant for $HO_2 + Kr$ listed in Table 1.

A similar spread in values exists for the NO_2 dissociation where two competing studies in Ar bath gas have been reported.[29,39] Estimates of the low-pressure limits have been made with the values from Rohrig et al.[29] being ∼1.8−2.6 times larger than those from Troe.[39] Which study is more accurate can be assessed by considering the direct measurements for the

reverse termolecular reaction, $O + NO + Ar$, by Yarwood et al.[40] These workers report $k_{O+NO+Ar} = 6.7 \times 10^{-32} \, T^{-1.41}$ cm^6 molecule^{-2} s^{-1} over the temperature range, 300−1341 K. The data from the two dissociation studies can be transformed using equilibrium constants, and as pointed out by Rohrig et al., the transformed values are within ±30% of the Yarwood et al. data. However, this conclusion was reached using JANAF[2] equilibrium constants for $NO_2 \leftrightarrow NO + O$, but as mentioned earlier in the previous paper in this issue,[3] ATcT now produces new and more accurate enthalpies of formation for NO_2 and NO. JANAF[2] lists $\Delta_f H_0°(NO) = 21.46 \pm 0.04$ kcal mol^{-1} (21.58 kcal mol^{-1} at 298 K) and $\Delta_f H_0°(NO_2) = 8.6 \pm 0.2$ kcal mol^{-1} (7.9 kcal mol^{-1} at 298 K), from which $\Delta_{Eq} H_0° = D_0(ON-O) = 71.9 \pm 0.2$ kcal mol^{-1} is obtained. As mentioned before, though the best currently available enthalpies of NO and NO_2 (from ATcT) are higher by ∼0.20 kcal mol^{-1} than those found in JANAF (and are now both known to be ±0.02 kcal mol^{-1}), the resulting $D_0(ON-O) = 71.85 \pm 0.03$ kcal mol^{-1} is very similar and, therefore, the changes from the JANAF equilibrium constants are fortuitously not large. This is shown in Figure 3
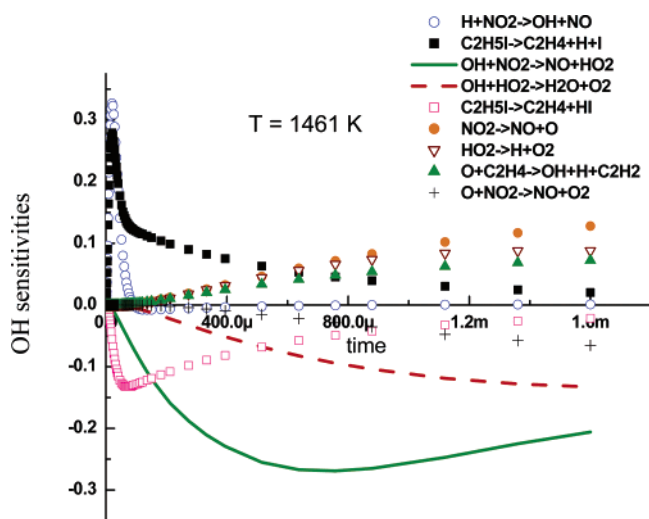
Figure 2. OH-radical sensitivity analysis for the profile shown in Figure 1 using the full reaction mechanism (Table 1) and the final fitted values of $k_{OH+NO_2} = 1.85 \times 10^{-12}$ and $k_{OH+HO_2} = 6 \times 10^{-11}$ both in cm^3 molecule^{-1} s^{-1}. The nine most sensitive reactions are shown in the inset.
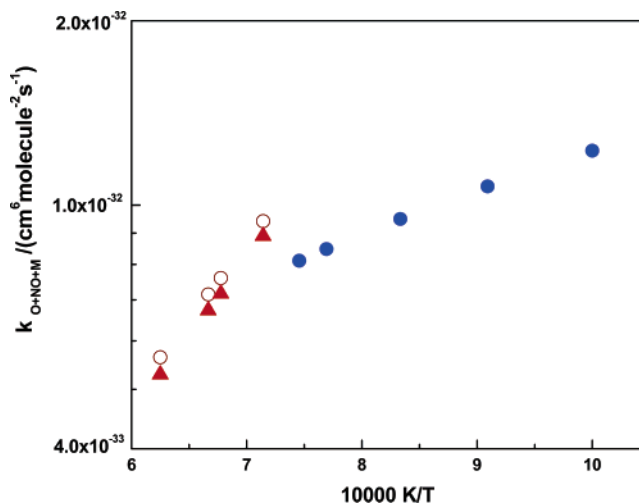
Figure 3. Third-order Arrhenius plot for the reaction $O + NO + M$: (●) ref 40 (300−1341 K); (▲) ref 29 using ref 2; (○) ref 29 using ATcT (for details see text).

Shock Tube Studies for Bimolecular Reactions

J. Phys. Chem. A, Vol. 110, No. 21, 2006 **6605**

TABLE 2: High-temperature Rate Data for OH + NO$_2$ and OH + HO$_2$

P_1/Torr	M_s[a]	$\rho_5/(10^{18}$ cm$^{-3})$[b]	T_5/K[b]	k_{OH+NO_2}[c]	k_{OH+HO_2}[c]
$X_{C_2H_5I} = 7.007 \times 10^{-6}$			$X_{NO_2} = 1.015 \times 10^{-4}$		
30.58	2.38	5.527	1407	1.35(−12)	7.50(−11)[d]
25.38	2.42	4.681	1449	1.30(−12)	3.31(−11)
20.99	2.39	3.815	1416	1.75(−12)	9.00(−11)
18.26	2.47	3.433	1502	2.25(−12)	8.00(−11)
15.95	2.27	2.758	1299	1.30(−12)	6.00(−11)
30.58	2.43	5.588	1461	1.85(−12)	6.00(−11)
30.13	2.21	4.981	1237	8.00(−13)	9.00(−11)
25.34	2.45	4.678	1486	2.40(−12)	1.00(−10)
17.84	2.38	3.217	1421	1.50(−12)	4.00(−11)
$X_{C_2H_5I} = 1.046 \times 10^{-5}$			$X_{NO_2} = 1.360 \times 10^{-4}$		
15.95	2.44	2.963	1482	1.63(−12)	9.50(−11)
15.90	2.27	2.736	1300	1.20(−12)	1.25(−10)
15.91	2.39	2.889	1423	1.35(−12)	9.30(−11)
15.87	2.36	2.846	1393	1.50(−12)	4.00(−11)
10.96	2.42	2.025	1462	2.20(−12)	3.80(−11)
10.91	2.38	1.981	1418	1.35(−12)	9.00(−11)
10.90	2.32	1.918	1357	1.15(−12)	8.00(−11)
10.87	2.48	2.062	1533	1.60(−12)	4.70(−11)
$X_{C_2H_5I} = 1.007 \times 10^{-5}$			$X_{NO_2} = 5.180 \times 10^{-5}$		
10.92	2.47	2.065	1511	2.10(−12)	6.00(−11)
15.96	2.40	2.912	1435	1.73(−12)	3.00(−11)
10.89	2.51	2.091	1554	2.10(−12)	8.50(−11)
10.93	2.43	2.039	1473	1.50(−12)	5.30(−11)
10.96	2.22	1.847	1254	1.40(−12)	6.20(−11)
10.99	2.30	1.930	1340	1.80(−12)	4.00(−11)
10.94	2.21	1.833	1242	9.00(−13)	4.00(−11)

[a] The error in measuring the Mach number, M_s, is typically 0.5−1.0% at the 1 std dev level giving ±1−2% uncertainty in ρ_5 and T_5. [b] Quantities with the subscript 5 refer to the thermodynamic state of the gas in the reflected shock region. [c] Rate constants in units cm^3 molecule^{-1} s^{-1}. [d] Parentheses denote the power of 10.

where the solid circles describing the third-order data of Yarwood et al.[40] are plotted along with the transformed data of Rohrig et al. using JANAF and ATcT equilibrium constant values, respectively. Clearly, the old and new values show good continuity with Yarwood et al. leading us to prefer the Rohrig et al. low-pressure result for the dissociation (Table 1).

The values for O + NO$_2$ and O + C$_2$H$_4$ listed in Table 1 are, respectively, from a recent study by Estupinan et al.[30] and evaluation by Baulch et al.[32] (coupled with the branching ratio results from Klemm et al.[33]). The rate constants for many of the 16 remaining reactions listed in Table 1 have either been measured or been evaluated in this laboratory.[13,15,16,26] In Figure 1, only two important unknown reactions out of the 16 are sensitive in determining [OH]$_t$. As shown in Figure 2, these are OH + NO$_2$ → NO + HO$_2$ and OH + HO$_2$ → O$_2$ + H$_2$O with the former being most important in the 200−600 μs regime while the latter contributes at later times. Note that the back reaction, NO + HO$_2$ → OH + NO$_2$, is also taken into account by using equilibrium constants, again from ATcT. Over the present temperature range, $K_{eq} = 4.353 \exp(-3571$ K/$T)$. With all other rate constants specified, both title reaction rate constants were varied to determine the best profile fit as shown in Figure 1. A profile fit with $k_{OH+NO_2} = 0$ is also plotted, indicating the importance of this reaction. Twenty-four experiments were performed between 1237 and 1554 K, and the conditions and resulting rate constant fits for both reactions are given in Table 2. Arrhenius plots are shown in Figures 4 and 5. For OH + NO$_2$ → NO + HO$_2$, varying rate constants by ±20% results in worse fits while the values for OH + HO$_2$ → O$_2$ + H$_2$O can vary by ±40% before poorer fits result. As seen in the inset of Figure 5, there is little evidence for temperature dependence for the OH + HO$_2$ reaction and the present results can be
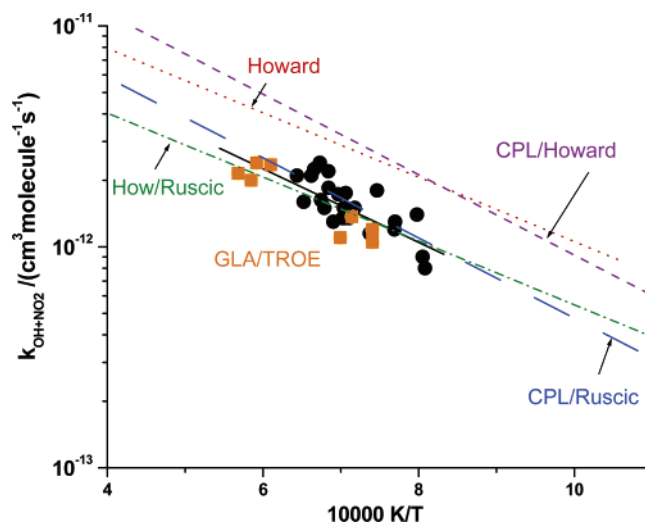
Figure 4. Arrhenius plot of the data for OH + NO$_2$ from Table 2: (●) present work (1237−1554 K); (■) ref 43, reanalyzed (see text); dotted line, ref 1; short dashed line, ref 41 (see text); long dashed line, ref 41 (see text); dash dots, ref 1 modified using ATcT (see text); thin solid line, eq 4 in the text.
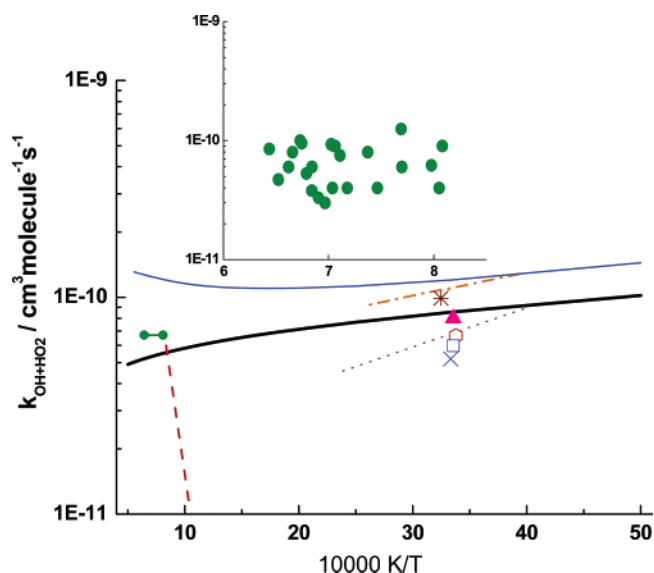
Figure 5. Arrhenius plot for OH + HO$_2$. Inset: (●) present work (1237−1554 K); Table 2. Full graph: thick solid line, ref 54; dash dots, ref 60; (*) ref 56; (▲) ref 61; dotted line, ref 58; (○) ref 57; (□) ref 59; (×) ref 7; dashed line, ref 48; thin solid line-collision theory (see text); (●−●) average of present work, $(6.7 \pm 2.6) \times 10^{-11}$ cm^3 molecule^{-1} s^{-1}.

represented as the average, $k_{OH+HO_2} = (6.7 \pm 2.6) \times 10^{-11}$ cm^3 molecule^{-1} s^{-1}.

The present values for k_{OH+NO_2} are compared to the discharge flow tube results of Howard[1] in Figure 4. In the figure, the extrapolation of the rate expression given by Howard is seen to be ∼2 times larger than the present data, as are the theoretical calculations of Chakraborty et al.[41] for the reverse reaction, transformed with equilibrium constants implied by Howard's data. However, if the data[1] and theory[41] for the back reaction, NO + HO$_2$, are transformed using equilibrium constants from the ATcT approach, the agreement with the present data is excellent. In a recent report,[42] a more accurate theoretical approach has been used to estimate the rate behavior; however, the results do not agree as well with experiment as the study by Chakraborty et al. There is one earlier experimental study on k_{OH+NO_2} at high temperature by Glaenzer and Troe[43] (GT).

These workers monitored HO_2 radicals in quite concentrated mixtures of HNO_3 and NO_2 in Ar bath gas, and they measured absolute $[HO_2]$ at half its maximum value and the associated decay time to reach this value. With assumptions for k_{OH+HO_2} and $k_{HO_2+NO_2}/k_{NO+HO_2}$, they could estimate values for k_{OH+NO_2} to within $\sim 30-40\%$.

Because the thermochemistry has changed appreciably since the work of GT, we have reanalyzed their results using the updated mechanism of Table 1 with the most important HO_2 destruction reaction, $HO_2 + NO_2$, included. Eight of their experiments were simulated by mutually varying both k_{OH+NO_2} and $k_{HO_2+NO_2}$ with a constant value of $k_{OH+HO_2} = 5 \times 10^{-11}$ cm^3 molecule^{-1} s^{-1} over their T range. This k_{OH+HO_2} value is a compromise between the present value and previous high-T measurements[44−48] that give values ranging from $\sim 1.8-10 \times 10^{-11}$ cm^3 molecule^{-1} s^{-1}. The reanalyzed values obtained from the simulations for k_{OH+NO_2} are plotted as solid squares in Figure 4 and are in excellent agreement with the present data. Recognizing that k_{OH+HO_2} is fairly uncertain, we performed a sensitivity analysis on this GT data[43] which shows that a $\pm 40\%$ change in OH + HO_2 results in $\pm 20\%$ and $\pm 30\%$ uncertainties in k_{OH+NO_2} and $k_{HO_2+NO_2}$, respectively.

If the present results are combined with the reanalyzed values from GT, then the rate constant for OH + NO_2 follows the Arrhenius expression

$$k_{OH+NO_2} =$$
$$2.25 \times 10^{-11} \exp(-3831 \text{ K}/T) \text{ cm}^3 \text{ molecule}^{-1} \text{ s}^{-1} \quad (4)$$

for the temperature range, 1200−1700 K. The derived rate constant for $HO_2 + NO_2$ over the GT T range from the simulations is, within experimental error, constant at $k_{HO_2+NO_2} = (2.2 \pm 0.7) \times 10^{-12}$ cm^3 molecule^{-1} s^{-1}.

There are no theoretical investigations for $k_{HO_2+NO_2}$ but several for k_{OH+HO2}.[49−55] Earlier determinations for $HO_2 + NO_2$ show that the reactivity at room temperature is strongly dominated by the third-order recombination reaction giving the stabilized product HO_2NO_2 and not $O_2 + HNO_2$. It is likely that the bimolecular products, first noted by GT, arise from competition, between forward and backward dissociations of vibrationally hot $HO_2NO_2^*$, and stabilization on a singlet potential energy surface. The most thorough ab initio electronic structure calculations on OH + HO_2 were carried out by Gonzalez et al. on both the singlet[54] and triplet surfaces.[55] They concluded that the singlet pathway through HOOOH was unimportant because the transition state was 15.2 kcal mol^{-1} higher lying than reactants. They identified tight transition states on the triplet surface corresponding to an abstraction pathway; however, the implied rate constants were much too low using transition state theory. They then calculated rate constants using a vibrationally/ rotationally adiabatic capture dipole−dipole model, but these values had to be scaled by 0.61 to make contact with existing low-temperature values[7,56−61] (ranging from 5.2 to 11.0 × 10^{-11} cm^3 molecule^{-1} s^{-1}). These experimental and theoretical values are plotted in Figure 5 along with the present determination. There are four studies at high temperature by Troe and co-workers[45−48] with the last being the preferred determination[48] (shown as the dashed line in Figure 5). These data imply a rapid increase in the rate constant, between ~ 1.2 and 7.0×10^{-11} cm^3 molecule^{-1} s^{-1}, for a small temperature increase, $\sim 970-$ 1220 K. This and earlier data[47] suggested a narrow minimum in the rate constant over a small T range with the minimum being at ~ 1000 K. There are no data in the intermediate T range, 420−950 K, to confirm this behavior, and the present data are not accurate enough to contribute to this question. Considering the difficulty in calculating ab initio surfaces as shown in previous work,[49−51,54,55] it may be difficult to theoretically justify such behavior using available electronic structure and dynamical methods. In past studies, we have employed a collision theory method to estimate bimolecular rate constants with no barriers,[62,63] and these are generally $\sim 60\%$ of better calculations that use accurate potential energy surfaces and flexible transition state theory.[64] The thin line in Figure 5 is a calculation assuming the triplet pathway for OH + HO_2 using collision theory, and this would be a rough upper estimate if no barrier exists for the reaction. The point to this illustration is that even if the narrow minimum exists at 1000 K, one would expect the bimolecular rate constant at high-T to level off at $\sim 1 \times 10^{-10}$ cm^3 molecule^{-1} s^{-1}. Hence, we conclude that the best available experimental value for OH + HO_2 in combustion modeling applications with $1200 \leq T \leq 1700$ K is $(5 \pm 3) \times 10^{-11}$ cm^3 molecule^{-1} s^{-1}.

4. Conclusions

On the basis of the ATcT approach, in the present work, we have used the best currently available values for the enthalpy of formation of HO_2, $\Delta_f H_0°(HO_2) = 3.64 \pm 0.06$ kcal mol^{-1} ($\Delta_f H_{298}°(HO_2) = 2.94 \pm 0.06$ kcal mol^{-1}), and new ATcT values for several other species, such as NO, NO_2, and OH. New kinetics measurements are reported confirming that the previous kinetics rate for OH + $NO_2 \rightarrow$ NO + HO_2 was too high by a factor of ~ 2. The new rate constant is $k_{OH+NO_2} = 2.25 \times 10^{-11} \exp(-3831 \text{ K}/T)$ cm^3 molecule^{-1} s^{-1} for the T range 1200−1700 K. We also conclude that the best available experimental value for OH + HO_2 in combustion modeling applications within $1200 \leq T \leq 1700$ K is $(5 \pm 3) \times 10^{-11}$ cm^3 molecule^{-1} s^{-1}. Simulating the experimental results of GT, we suggest that $k_{HO_2+NO_2}$ over the T range 1350−1760 K is constant at $(2.2 \pm 0.7) \times 10^{-11}$ cm^3 molecule^{-1} s^{-1}.

References and Notes

(1) Howard, C. J. *J. Am. Chem. Soc.* **1980**, *102*, 6937.
(2) Chase, M. W., Jr.; Davies, C. A.; Downey, J. R., Jr.; Frurip, D. J.; McDonald, R. A.; Syverud, A. N. *J. Phys. Chem. Ref. Data* **1985**, *14*, Suppl. 1. Chase, M. W., Jr. *J. Phys. Chem. Ref. Data* **1998**, Monograph 9.
(3) Ruscic, B.; Pinzon, R. E.; Morton, M. E.; Srinivasan, N. K.; Su, M.-C.; Sutherland, J. W.; Michael, J. V. *J. Phys. Chem. A* **2006**, *110*, 6592.
(4) DeMore, W. B.; Sander, S. P.; Golden, D. M.; Hampson, R. F.; Kurylo, M. J.; Howard, C. J.; Ravishankara, A. R.; Kolb, C. E.; Molina, M. J. *Chemical Kinetics and Photochemical Data for Use in Stratospheric Modeling*; Evaluation No. 12 JPL Publication 97-4; Jet Propulsion Laboratory: Pasadena, CA, 1997.
(5) Hack, W.; Preuss, A. W.; Temps, F.; Wagner, H. Gg.; Hoyermann, K. *Int. J. Chem. Kinet.* **1980**, *12*, 851.
(6) Thrush, B. A.; Wilkinson, J. P. T. *Chem. Phys. Lett.* **1981**, *81*, 1.

Shock Tube Studies for Bimolecular Reactions

J. Phys. Chem. A, Vol. 110, No. 21, 2006 **6607**

(7) Rozenshtein, V. B.; Gershenzon, Yu. M.; Il'in, S. D.; Kishkovitch, O. P. *Chem. Phys. Lett.* **1984**, *112*, 473.

(8) Jemi-Alade, A. A.; Thrush, B. A. *J. Chem. Soc., Faraday Trans.* **1990**, *86*, 3355.

(9) Seeley, J. V.; Meads, R. F.; Elrod, M. J.; Molina, M. J. *J. Phys. Chem.* **1996**, *100*, 4026.

(10) Bohn, B.; Zetzsch, C. *J. Chem. Soc., Faraday Trans.* **1998**, *94*, 1203.

(11) Srinivasan, N. K.; Su, M.-C.; Sutherland, J. W.; Michael, J. V. *J. Phys. Chem. A* **2005**, *109*, 1857.

(12) Su, M.-C.; Kumaran, S. S.; Lim, K. P.; Michael, J. V. *Rev. Sci. Instrum.* **1995**, *66*, 4649.

(13) Su, M.-C.; Kumaran, S. S.; Lim, K. P.; Michael, J. V.; Wagner, A. F.; Harding, L. B.; Fang, D.-C. *J. Phys. Chem. A* **2002**, *106*, 8261.

(14) Srinivasan, N. K.; Su, M.-C.; Sutherland, J. W.; Michael, J. V. *J. Phys. Chem. A* **2005**, *109*, 7902.

(15) Kumaran, S. S.; Su, M.-C.; Lim, K. P.; Michael, J. V. *Proc. Combust. Inst.* **1996**, *26*, 605.

(16) Michael, J. V. *Prog. Energy Combust. Sci.* **1992**, *18*, 327.

(17) Michael, J. V. In *Advances in Chemical Kinetics and Dynamics*; Barker, J. R., Ed.; JAI Press: Greenwich, CT, 1992; Vol. I, pp 47−112, for original references.

(18) Michael, J. V.; Kumaran, S. S.; Su, M.-C. *J. Phys. Chem. A* **2000**, *104*, 980.

(19) Michael, J. V.; Sutherland, J. W. *Int. J. Chem. Kinet.* **1986**, *18*, 409.

(20) Michael, J. V. *J. Chem. Phys.* **1989**, *90*, 189.

(21) Michael, J. V.; Fisher, J. R. In *Seventeenth International Symposium on Shock Waves and Shock Tubes*; Kim, Y. W., Ed.; AIP Conference Proceedings 208; American Institute of Physics: New York, 1990; pp 210−215.

(22) Krasnoperov, L. N.; Michael, J. V. *J. Phys. Chem. A* **2004**, *108*, 5643.

(23) Wooldridge, M. S.; Hanson, R. K.; Bowman, C. T. *Int. J. Chem. Kinet.* **1994**, *26*, 389.

(24) Ruscic, B.; Wagner, A. F.; Harding, L. B.; Asher, R. L.; Feller, D.; Dixon, D. A.; Peterson, K. A.; Song, Y.; Qian, X.; Ng, C. Y.; Liu, J.; Chen, W.; Schwenke, D. W. *J. Phys. Chem. A* **2002**, *106*, 2727.

(25) Herbon, J. T.; Hanson, R. K.; Golden, D. M.; Bowman, C. T. *Proc. Combust. Inst.* **2002**, *29*, 1201.

(26) Michael, J. V.; Kumaran, S. S.; Su, M.-C.; Lim, K. P. *Chem. Phys. Lett.* **2000**, *319*, 99.

(27) Du, H.; Hessler, J. P. *J. Chem. Phys.* **1992**, *96*, 1077.

(28) Oldenborg, R. C.; Loge, G. W.; Harradine, D. M.; Winn, K. R. *J. Phys. Chem.* **1992**, *96*, 8426.

(29) Rohrig, M.; Petersen, E. L.; Davidson, D. F.; Hanson, R. K. *Int. J. Chem. Kinet.* **1997**, *29*, 483.

(30) Estupinan, E. G.; Nicovich, J. M.; Wine, P. H. *J. Phys. Chem. A* **2001**, *105*, 9697.

(31) Tully, F. P. *Chem. Phys. Lett.* **1988**, *143*, 510.

(32) Baulch, D. L.; Cobos, C. J.; Cox, R. A.; Frank, P.; Hayman, G.; Just, Th.; Kerr, J. A.; Murrells, T.; Pilling, M. J.; Troe, J.; Walker, R. W.; Warnatz, J. *J. Phys. Chem. Ref. Data* **1994**, *23*, 847.

(33) Klemm, R. B.; Sutherland, J. W.; Wickramaaratchi, M. A.; Yarwood, G. *J. Phys. Chem.* **1990**, *94*, 3354.

(34) Michael, J. V.; Su, M.-C.; Sutherland, J. W.; Carroll, J. J.; Wagner, A. F. *J. Phys. Chem. A* **2002**, *106*, 5297.

(35) Jenkin, M. E.; Cox, R. A.; Mellouki, A.; Le Bras, G.; Poulet, G. *J. Phys. Chem.* **1990**, *94*, 2927.

(36) Tsang, W.; Hampson, R. F. *J. Phys. Chem. Ref. Data* **1986**, *15*, 1087.

(37) http://www.me.berkeley.edu/gri_mech/.

(38) http://chem.leeds.ac.uk/combustion/combustion.html/.

(39) Troe, J. *Ber. Bunsen-Ges. Phys. Chem.* **1969**, *73*, 144.

(40) Yarwood, G.; Sutherland, J. W.; Wickramaaratchi, M. A.; Klemm, R. B. *J. Phys. Chem.* **1991**, *95*, 8771.

(41) Chakraborty, D.; Park, J.; Lin, M. C. *Chem. Phys.* **1998**, *231*, 39.

(42) Zhu, R. S.; Lin, M. C. *J. Chem. Phys.* **2003**, *119*, 10667.

(43) Glaenzer, K.; Troe, J. *Ber. Bunsen-Ges. Phys. Chem.* **1975**, *79*, 465.

(44) Goodings, J. N.; Hayhurst, A. N. *J. Chem. Soc., Faraday Trans. 2* **1988**, *84*, 745.

(45) Hippler, H.; Troe, J. *J. Chem. Phys.* **1990**, *93*, 1755.

(46) Hippler, H.; Troe, J. *Chem. Phys. Lett.* **1992**, *192*, 333.

(47) Hippler, H.; Neunaber, H.; Troe, J. *J. Chem. Phys.* **1995**, *103*, 3510.

(48) Kappel, Ch.; Luther, K.; Troe, J. *Phys. Chem. Chem. Phys.* **2002**, *4*, 4392.

(49) Cremer, D. *J. Chem. Phys.* **1978**, *69*, 4456.

(50) Jackels, C. F.; Phillips, D. H. *J. Chem. Phys.* **1986**, *84*, 5013.

(51) Toohey, D. W.; Anderson, J. G. *J. Phys. Chem.* **1989**, *93*, 1094.

(52) Mozurkewich, M. *J. Phys. Chem.* **1986**, *90*, 2216.

(53) Phillips, L. F. *J. Phys. Chem.* **1990**, *94*, 7482.

(54) Gonzalez, C.; Theisen, J.; Zhu, L.; Schlegel, H. B.; Hase, W. L.; Kaiser, E. W. *J. Phys. Chem.* **1991**, *95*, 6784.

(55) Gonzalez, C.; Theisen, J.; Schlegel, H. B.; Hase, W. L.; Kaiser, E. W. *J. Phys. Chem.* **1992**, *96*, 1767.

(56) Cox, R. A.; Burrows, J. P.; Wallington, R. J. *Chem. Phys. Lett.* **1981**, *84*, 217.

(57) Temps, F.; Wagner, H. Gg. *Ber. Bunsen-Ges. Phys. Chem.* **1982**, *86*, 119.

(58) Sridharan, U. C.; Qiu, L. X.; Kaufman, F. *J. Phys. Chem.* **1984**, *88*, 1281.

(59) Dransfeld, P.; Wagner, H. Gg. *Z. Naturforsch. A: Phys. Sci.* **1987**, *42*, 471.

(60) Keyser, L. F. *J. Phys. Chem.* **1988**, *92*, 1193.

(61) Schwab, J. J.; Brune, W. H.; Anderson, J. G. *J. Phys. Chem.* **1989**, *93*, 1030.

(62) Kumaran, S. S.; Su, M.-C.; Lim, K. P.; Michael, J. V.; Wagner, A. F.; Harding, L. B. *J. Phys. Chem.* **1996**, *100*, 7541.

(63) Sutherland, J. W.; Su, M.-C.; Michael, J. V. *Int. J. Chem. Kinet.* **2001**, *33*, 669.

(64) *VARIFLEX*, version 1.0 (http://chemistry.anl.gov/chem-dyn/Vari-Flex), VARIFLEX is a freeware program package for calculating gas-phase reaction rates written by Klippenstein, S. J.; Wagner, A. F.; Robertson, S. H.; Dunbar, R. C.; Wardlaw, D. M. in 1999.

(65) http://cmcs.org

(66) http://www.iupac.org/projects/2003/2003-024-1-100.html